Computation of Cutoff Wavenumbers for Partially Filled Waveguides of Arbitrary Cross Section Using Surface Integral Formulations and the Method of Moments

Shianfeng Shu, Paul M. Goggans, and Ahmed A. Kishk

Abstract—**A procedure for determining the cutoff wavenumbers of partially dielectric filled waveguides of arbitrary cross section is presented. A numerical approach based on surface integral formulations and the method of moments is used to obtain a matrix equation. Muller's method is then applied to find the wavenumbers that make the matrix determinant vanish. These are the cutoff wavenumbers. On the conducting walls of the waveguide, perfect electric conductor, perfect magnetic conductor, and imperfect conductor surfaces are considered. The transverse electric and magnetic cases are treated separately. The impedance boundary condition and the symmetry of the waveguide cross section are used to reduce the matrix size in the method of moments. Spurious modes have not been observed using this method. To validate the accuracy of this method, results for circular, partially filled rectangular, and two walled corrugated rectangular waveguides are compared to analytical results. Examples such as T-septate rectangular, coaxial, and dielectric-loaded double-ridged waveguide are also considered. Accurate prediction on the cutoff wavenumbers is achieved.**

I. Introduction

The problem of electromagnetic wave propagation inside waveguides of arbitrary cross section has been the subject of many research works over the last two decades [1]–[10]. A variety of numerical approximation methods has been employed [1]. The early methods frequently suffer from the appearance of nonphysical or spurious modes [4]. Recently, several papers [5]–[9] proposed methods without spurious solutions. Among these methods are the finite element method (FEM) and the method of moments (MM).

These two methods each have properties which makes the use of one or the other advantageous depending on nature of the waveguide and the desired computational result. Due to its surface formulation, the MM cannot easily model materials with a rapid spatial variation of constitutive parameters. Because of its volumetric formulation, the FEM is the method to choose when treating waveguides filled with truly inhomogeneous material. If, however, the inhomogeneous region is composed of a few distinct subregions, each with constant material parameters, the MM can be employed and may result in fewer computations than required in the FEM solution. Because it is cast in terms of the field components, the finite element method may be the best choice if field components are desired. Similarly, the MM is formulated in terms of the equivalent surface currents on the waveguide boundaries and so may be the best choice if currents are desired. Of course, either method can calculate currents and fields with auxiliary computations. A practical point to consider is that research in the FEM solution of waveguide problems is more mature than research in MM solutions.

Several authors have successfully solved the problem of hollow waveguide of arbitrary cross section with perfect electric conductor walls using the MM [8], [9]; however, the problem of waveguides partially filled with dielectric and with impedance walls has not yet been fully investigated. Here we use the MM to determine the cutoff wavenumbers of partially filled waveguides with impedance surfaces.

The size of the MM impedance matrix is much greater for a waveguide with a dielectric filling than for identically shaped hollow waveguide. This is because, on the dielectric interface, the equivalent electric and magnetic currents must be determined in addition to the equivalent electric current on the conductor surfaces. Excessive execution time and memory storage requirements are among the problems caused by large matrix size. For a matrix of order N, the inversion time is of order N^3 and the required storage area is of order N^2. Another serious problem associated with large matrix size is that the behavior of the determinant as a function of the wavenumber becomes more complicated as N increases. The null points of the determinant versus the wavenumber are the desired cutoff wavenumbers. A typical plot of the magnitude of the determinant versus the wavenumber is given in Fig. 1. The valleys around the null points become much narrower and sharper as the matrix size increases [9]. For large matrices, it is very difficult to locate the null points and the cutoff wavenumbers can be easily missed.

The size of the MM impedance matrix can be reduced in several ways. Since the MM is formulated in terms of equivalent currents on the boundary surfaces, any other method that yields a direct approximation to these currents, or a relationship between these currents, can be combined with it to reduce the number of unknowns. Such methods are

Manuscript received February 10, 1992; revised October 20, 1992. This work was supported by the National Science Foundation under Grant ECS-9015328.

S. Shu is with Formosa Plastics Corporation, USA, 9 Peach Tree Hill Road, Livingston, NJ 07039.

P. M. Goggans and A. A. Kishk are with the Department of Electrical Engineering, University of Mississippi University, MS 38677.

IEEE Log Number 9209334.

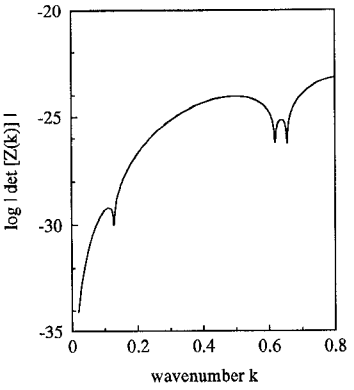

Fig. 1. Behavior of determinant of impedance matrix for the dielectric-loaded double-ridged waveguide.

referred to as hybrid or combined methods. For example, the impedance boundary condition (IBC) can be used to relate the equivalent magnetic currents to the equivalent electric currents on some surface boundaries to reduce significantly the matrix size. The impedance boundary condition is typically applied to corrugated surfaces and imperfectly conducting surfaces. The matrix size can further be reduced by considering the symmetry of the waveguide.

II. Formulations

Fig. 2 illustrates the general geometry of an arbitrary cross-section waveguide partially filled with dielectric. For this geometry, there are three distinct regions: R_c, R_e, and R_d. Region R_c is conductor exterior to the waveguide, region R_e is empty space characterized by permittivity ϵ_0 and permeability μ_0, and region R_d is the homogenous dielectric region characterized by permittivity ϵ_d and permeability μ_d. The conductor surfaces may consist of perfect electric conductor (PEC), perfect magnetic conductor (PMC), and/or imperfect conductor (IC) where the IBC is applied. In the following, $\boldsymbol{J}_\beta^\alpha$ and $\boldsymbol{M}_\beta^\alpha$ are, respectively, the electric and the magnetic surface currents, and S_β^α denotes the surfaces of the boundaries. The superscript α denotes the type of conductor and the subscript β denotes the surface. The superscripts are defined as follows: (i) denotes an IC boundary, (m) denotes a PMC boundary, and (e) denotes a PEC boundary. The subscripts are defined as follows: (ce) denotes the boundary surface between the conductor and empty space, (cd) denotes the boundary surface between the conductor and dielectric, and (d) denotes the boundary surface between the dielectric and empty space. So, S_{ce}, S_d, and S_{cd} are the waveguide boundaries. For the purposes of developing the MM expressions, it is assumed that source currents exist in $\boldsymbol{R}_e$. The symbols $\boldsymbol{J}_i$ and $\boldsymbol{M}_i$ denote source currents. The fields $\boldsymbol{E}_0$ and $\boldsymbol{H}_0$ are the electric and magnetic fields in $\boldsymbol{R}_e$, and $\boldsymbol{E}_d$ and $\boldsymbol{H}_d$ are the electric and magnetic fields in $\boldsymbol{R}_d$. The unit normal vector on the surfaces is denoted by $\hat{\boldsymbol{n}}$.

The boundary conditions are as follows: the tangential component of the electric field is zero on PEC, the tangential component of the magnetic field is zero on PMC, the electric and magnetic fields are continuous across the dielectric/free-space interface. On IC, the following condition (the impedance boundary condition) is assumed:

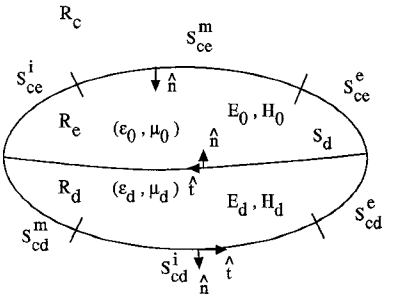

Fig. 2. The original problem for waveguides partially filled with dielectric.

$$\boldsymbol{E}_\nu - (\hat{\boldsymbol{n}} \cdot \boldsymbol{E}_\nu)\hat{\boldsymbol{n}} = \eta_{c\nu}\eta_0(\hat{\boldsymbol{n}} \times \boldsymbol{H}_\nu) \qquad \text{on } S_{c\nu}^i \ (\nu = e \text{ or } d) \tag{1}$$

where η_0, η_{ce}, and η_{cd} are the intrinsic impedance of the space, the surface impedance on S_{cd}^i, and the surface impedance on S_{cd}^i, respectively.

Applying the equivalence principal [11], two auxiliary problems are created from the original problem (Figs. 3 and 4). One situation is equivalent to the original problem in empty space (region R_c, between S_{ce} and S_d), and the other is equivalent to the original problem inside the dielectric (region R_d between S_d and S_{cd}). The surface equivalent currents are defined as follows:

$$\boldsymbol{J}_p^q = (\pm\hat{\boldsymbol{n}}) \times \boldsymbol{H}_\nu \qquad \text{on } S_p^q \ (q = i \text{ or } e) \tag{2}$$

$$\boldsymbol{M}_p^q = \boldsymbol{E}_\nu \times (\pm\hat{\boldsymbol{n}}) \qquad \text{on } S_p^q \ (q = i \text{ or } m) \tag{3}$$

where p is ce, cd, or d, ν is 0 or d, and the sign of the normal is $+$ for $\nu = 0$ and $-$ for $\nu = d$.

Using the impedance boundary condition given in (1), the equivalent magnetic surface currents can be expressed in terms of the equivalent electric surface currents on S_{ce}^i.

$$\boldsymbol{M}_p^i = \eta_p\eta_0\left(\boldsymbol{J}_p^i \times \hat{\boldsymbol{n}}\right) \qquad \text{on } S_p^n \ (p \text{ is } ce \text{ or } cd). \tag{4}$$

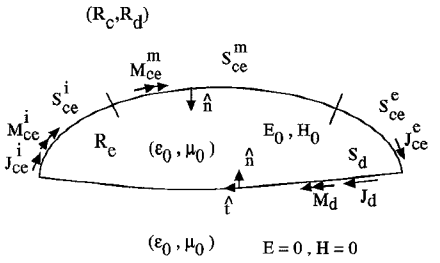

Fig. 3. The empty space equivalent situation.

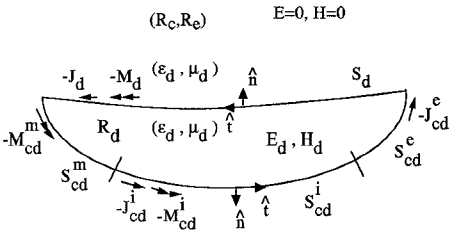

Fig. 4. The dielectric region equivalent situation.

In the zero field regions, the constitutive parameters are taken to be the same as in the nonzero field region, so that the equivalent currents radiate in an unbounded homogeneous region. The tangential components of $\boldsymbol{E}$ and $\boldsymbol{H}$ must be zero just outside S_{ce} and S_d so that:

$$\boldsymbol{E}_{\tan}(\boldsymbol{J}_i, \boldsymbol{M}_i) + \boldsymbol{E}_{\tan}(\boldsymbol{J}^e_{ce}) + \boldsymbol{E}_{\tan}(\boldsymbol{J}^i_{ce}, \boldsymbol{M}^i_{ce}) + \boldsymbol{E}_{\tan}(\boldsymbol{M}^m_{ce}) + \boldsymbol{E}_{\tan}(\boldsymbol{J}_d, \boldsymbol{M}_d) = 0 \quad \text{just outside } S_{ce} \text{ and } S_d \tag{5}$$

$$\hat{\boldsymbol{n}} \times \boldsymbol{H}(\boldsymbol{J}_i, \boldsymbol{M}_i) + \hat{\boldsymbol{n}} \times \boldsymbol{H}(\boldsymbol{J}^e_{ce}) + \hat{\boldsymbol{n}} \times \boldsymbol{H}(\boldsymbol{J}^i_{ce}, \boldsymbol{M}^i_{ce}) + \hat{\boldsymbol{n}} \times \boldsymbol{H}(\boldsymbol{M}^m_{ce}) + \hat{\boldsymbol{n}} \times \boldsymbol{H}(\boldsymbol{J}_d, \boldsymbol{M}_d) = 0 \quad \text{just outside } S_{ce} \text{ and } S_d \tag{6}$$

$$\boldsymbol{E}_{\tan}(\boldsymbol{J}^e_{cd}) - \boldsymbol{E}_{\tan}(\boldsymbol{J}^i_{cd} + \boldsymbol{M}^i_{cd}) - \boldsymbol{E}_{\tan}(\boldsymbol{M}^m_{cd}) - \boldsymbol{E}_{\tan}(\boldsymbol{J}_d, \boldsymbol{M}_d) = 0 \quad \text{just outside } S_{cd} \text{ and } S_d \tag{7}$$

$$-\hat{\boldsymbol{n}} \times \boldsymbol{H}(\boldsymbol{J}^e_{cd}) - \hat{\boldsymbol{n}} \times \boldsymbol{H}(\boldsymbol{J}^i_{cd}, \boldsymbol{M}^i_{cd}) - \hat{\boldsymbol{n}} \times \boldsymbol{H}(\boldsymbol{M}^m_{cd}) - \hat{\boldsymbol{n}} \times \boldsymbol{H}(\boldsymbol{J}_d, \boldsymbol{M}_d) = 0 \quad \text{just outside } S_{cd} \text{ and } S_d \tag{8}$$

where

$$\boldsymbol{E}_{\tan} = -\hat{\boldsymbol{n}} \times \hat{\boldsymbol{n}} \times \boldsymbol{E}\,. \tag{9}$$

Equations (5) and (7) express the electric field boundary condition in the region R_e and the region R_d of the equivalent situations. These two equations form a set of integral equations known as the electric field integral equation (EFIE).

Equations (6) and (8) express the magnetic field boundary conditions in region R_e and region R_d of equivalent situations. These two equations form a set of integral equations known as the magnetic field integral equation (MFIE).

A new set of integral equation can be obtained by combining the equations of the EFIE and the MFIE. This new set of equations is referred to as the combined field integral equation (CFIE). To obtain the equations of CFIE, the equations of the EFIE are multiplied by dimensional and scaling factor and then added to the equations of the MFIE. The equations of the CFIE are MFIE $\pm\alpha$EFIE$/\eta_0$ (+ for the inside equations and $-$ for the outside equations). The dimensional constant η_0 is required so that the dimensions of the EFIE match those of the MFIE. In principle, the value of scaling factor α is arbitrary as long as the real part of α is positive (usually α is real and on the order of unity). In practice, the numerical results are relatively insensitive to α.

In general, the analysis of waveguides is a three-dimensional problem. However, at cutoff frequencies, it is a two-dimensional problem because there are no propagating waves. As a result, the cutoff wavenumbers can be determined from the two-dimensional problem. Because the waveguide is a 2-D problem at cutoff, an arbitrarily polarized wave can always be written as the combination of waves that are transverse electric (TE) and transverse magnetic (TM) to the axis of the waveguide (here taken to be the z direction).

In the TM case at cutoff, the equivalent electric currents are all axially directed and the equivalent magnetic currents are circumferentially directed. The equivalent currents can be written in the following form:

$$\boldsymbol{J}^q_p = J^q_p \hat{\boldsymbol{z}} \tag{10}$$

$$\boldsymbol{M}^q_p = M^q_p \hat{\boldsymbol{t}} \tag{11}$$

where p stands for (ce), (cd), or (d), and q stands for (i), (e), or (m). The position for q is left blank when p is d. In these expressions, $\hat{\boldsymbol{z}}$ and $\hat{\boldsymbol{t}}$ are unit vectors in z direction and the tangential direction, respectively, and

$$\hat{\boldsymbol{t}} = \hat{\boldsymbol{z}} \times \hat{\boldsymbol{n}}\,. \tag{12}$$

Specializing (4) to the TM case, results in the following equation:

$$M^i_p \hat{\boldsymbol{t}} = \eta_p \eta_0 J^i_p \hat{\boldsymbol{t}} \qquad \text{on } S^i_p \ (p \text{ is } ce \text{ or } cd)\,. \tag{13}$$

The currents in (10), (11), and (13) give rise to TM fields only. If these currents are substituted into (5)–(8), the scaler integral equations for the TM case are obtained.

In the TE case at cutoff, the equivalent electric currents are all circumferentially directed and the equivalent magnetic currents are axially directed. The procedure for obtaining the scaler integral equations for the TE case is similar to that for the TM case.

III. Method of Moments

To apply the MM, the boundaries of the waveguide are divided into segments. Here, a piecewise linear approximation of the boundaries of the waveguide is made. The surface currents are expanded on each segment in terms of pulse functions. Then the point matching method is employed on the center of each segment. This method results in a system of linear equations in terms of unknown coefficients.

For the TM case, the equivalent currents are expanded as

$$\boldsymbol{J}^q_p = \hat{\boldsymbol{z}} \sum_n I_n P_n \qquad \text{on } S^q_p (p \text{ is } ce, cd \text{ or } d, q \text{ is } e \text{ or } m) \tag{14}$$

and

$$\boldsymbol{M}^q_p = \sum_n \hat{\boldsymbol{t}}_n K_n P_n \qquad \text{on } S^q_p (p \text{ is } ce, cd \text{ or } d, q \text{ is } m)\,. \tag{15}$$

In (14) and (15), I_n and K_n are the to-be-determined electric and magnetic current expansion coefficients, and the P_n are the pulse expansion functions. The vector $\hat{\boldsymbol{t}}_n$ is the unit tangent on zone n. From (13), the magnetic currents on the IBC surfaces are

$$M^i_p = \sum_n \hat{\boldsymbol{t}}_n \eta_p \eta_0 I_n P_n (p \text{ is } ce \text{ or } cd)\,. \tag{16}$$

If the above equations are substituted into scaler equations for TM case and the resulting expressions are required to be satisfied at the matching points, the original problem can be reduced to a matrix equation of the form

$$[Z(k)][J] = [V]\,. \tag{17}$$

In (17), Z is a square matrix of order $n_{ce}^{\text{tot}} + 2n_d + n_{cd}^{\text{tot}}$ where, n_{ce}^{tot}, n_d^{tot}, and n_{cd}^{tot} are the numbers of segments on S_{ce}, S_d, and S_{cd}, respectively. Expressions for the generalized impedance elements of $[Z(k)]$ are given in [12].

For the TE case, the procedure of applying MM is similar to that in TM case. The impedance elements in the TE case can be derived by using duality from the impedance elements in the TM case.

At cutoff, no incident wave is necessary to produce the fields inside the waveguide, the matrix Z is singular and the determinant of the matrix Z is zero. As a result, the cutoff wavenumbers are characterized by

$$\det[Z(k_c)] = 0\,. \tag{18}$$

The determinant in (18) can be determined using the LU decomposition method [13].

In the method of moments, the expansion set of the equivalent currents is not complete, so the absolute value of the matrix determinant cannot be exactly zero. As a function of k, the matrix determinant shows a set of minimums instead. The values of k, where the minimums occur, are the approximate cutoff wavenumbers. The locations of the minimums are here determined by Muller's method. Initial guesses for the values of the cutoff wavenumbers are obtained by scanning the range of k values of interest with the body discretized into relatively large segments (approximately one-fifth wavelength zones). The body is then discretized into relatively small segments (approximately one-twentieth wavelength zones) and Muller's method is used for each guess. The larger the number of the segments taken in the MM solution, the more exactly the cutoff wavenumbers can be obtained. At cutoff, the smallest eigenvalue of $[Z(K_c)]$, $\lambda_{\min}$, corresponds to the wavenumber in the z direction. It is not zero because of the incomplete expansion of the wall currents. The eigenvector of the MM matrix corresponding to $\lambda_{\min}$ is an approximation of the wall currents at cutoff.

IV. Numerical Examples

A numerical code was developed on the Cray-XMP supercomputer. Using this code, the cutoff wavenumbers of several typical geometries were calculated. Results generated with this code are presented in this section. First, some geometries with analytical solutions are considered. Then, more complicated geometries are considered and the results are compared to those obtained by other authors. Finally, a new ridged waveguide with dielectric loading and corrugated surfaces is considered and the results are discussed.

A. Circular Waveguide

As a first example, a hollow circular waveguide is considered. This example is the test case for curved boundaries. In Table I, the computed results (both TE and TM case) are compared with the exact results. The MFIE is used for this geometry. The circular boundary is divided into thirty segments. The largest difference between the computed values and the exact values given in Table I is less than 0.5%.

TABLE I
Cutoff Wavenumbers for the Hollow Circular Waveguide with Unity Radius

TM		TE	
Exact	Computed	Exact	Computed
2.4048	2.4108	1.8412	1.8449
3.8317	3.8382	3.0542	3.0629
5.1356	5.1429	3.8317	3.8356
5.5200	5.5272	4.2012	4.2164

B. Partially Dielectric Filled Rectangular Waveguide

As a numerical example of partially dielectric filled waveguides, the waveguide shown in Fig. 5(a) was investigated. Half the waveguide is filled with dielectric with relative permittivity equal to 1.5. The other half is assumed to be vacuum. The exact solution for this geometry is given in [15]. Above cutoff, independent modes TE to x or TM to x exist in this waveguide. At cutoff, modes TE to x correspond to modes TM to z and modes TM to x correspond to modes TE to z. In Table II, the computed results are compared to the exact solutions. Here, the matrix is of order 102 and the MFIE is used. The largest error in Table II is less than 0.1%. Note that the boundary of the dielectric region must be divided according to the wavelength in the dielectric material to achieve accurate solutions.

C. Half of the Partially Filled Rectangular Waveguide

For the case above, the symmetry of the waveguide can be advantageously considered to reduce the matrix size. As illustrated in Fig. 5(b), the symmetry plane is denoted as PP′. At cutoff, the original problem can be subdivided into four distinct cases: TM or TE to z modes with PEC or PMC walls at PP′. The PEC wall provides the cutoff wavenumber

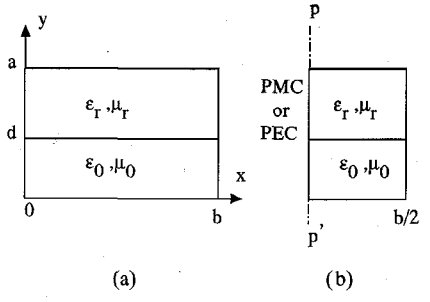

Fig. 5. (a) Partially dielectric filled rectangular waveguide. For this example $\mu_r = 1.0$, $\epsilon_r = 1.5$, $a = 0.45$, $b = 1.0$, and $d = 0.225$. (b) Half of the partially filled rectangular waveguide.

TABLE II
Cutoff Wavenumbers for Partially Filled Rectangular Waveguide

TM		TE	
Exact	Computed	Exact	Computed
6.8072	6.8086	6.2136	6.2145
8.3277	8.3259	6.8356	6.8379
10.3522	10.3409	8.4665	8.4694
12.6140	12.5882	10.7253	10.7295

TABLE III
CUTOFF WAVENUMBERS FOR PARTIALLY DIELECTRIC FILLED RECTANGULAR WAVEGUIDE (HALF) TM

Exact	(PMC*) Computed	(PEC*) Computed
6.8072		6.7971
8.3277	8.3172	
10.3522		10.3274
12.6140	12.5699	
12.9932		12.9683

*PMC and PEC denote the wall of symmetry.

corresponding to the modes that have zero tangential electric field on the plane of symmetry of the original problem. On the other hand, the PMC wall provides the cutoff wavenumbers corresponding to modes that have zero tangential magnetic field on the plane of symmetry of the original problem. If the cutoff wavenumber is the same for PEC wall and PMC wall cases, it means that the tangent electric and magnetic fields are both zero on the plane of symmetry.

In Table III, the symmetry of the waveguide has been used to replace the plane of symmetry with a PEC or PMC wall. The results in Table III are for the TM to z (TE to x) case. For the purpose of comparison, the length of the zones remained unchanged when symmetry was considered. The matrix order using symmetry is 58 (it was 102 before). The EFIE was used for the case of the PEC at the plane of symmetry, and the MFIE was used for the case of the PMC at the plane of symmetry. The error of the computed values in Table III is then 0.2% (compared to 0.1% before). Using symmetry, the matrix size is reduced and the accuracy remains at an acceptable level. Accuracy matching the previous result can be achieved using smaller zone size with the waveguide symmetry. Reducing the zone size to increase accuracy while using symmetry still results in reduced matrix order compared to solving the complete problem.

D. T-Septate Rectangular Waveguide

The T-septate rectangular waveguide, illustrated in Fig. 6, has been considered by many investigators. The current method can be used for this geometry because pulse expansion functions and point matching method are employed in the MM (the matching points need not be at the junctions of the T-septate). For this waveguide, the EFIE is used because the T-septate is assumed to be infinitesimally thin. The results of the present method are compared to those of [7] in Table IV. In [7], the finite difference time domain method was used to find the cutoff wavenumber. The matrix in the present method was of order 64. The largest difference in Table IV is about 1.0%.

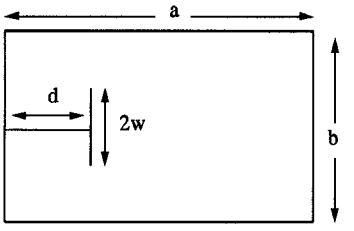

Fig. 6. T-septate rectangular waveguide. For this example, $a = 1.0$, $b = 0.45$, $d = 0.25$, and $w = 0.125$.

TABLE IV
CUTOFF WAVENUMBERS FOR THE T-SEPTATE RECTANGULAR WAVEGUIDE

TM		TE	
Reference [7]	Present	Reference [7]	Present
8.12	8.1302	3.00	3.0015
10.88	10.8720	5.49	5.4265
14.24	14.3124	7.22	7.2252
14.50	14.5439	8.88	8.8625

E. Coaxial Waveguide

Fig. 7 shows a coaxial waveguide with a rectangular conducting core and circular conducting exterior boundary. In Table V, the solutions of this example are compared to the values obtained by Swaminathan *et al.* [9] using surface integral formulations also. The largest difference is about 1.0%. The EFIE is used here. The matrix size is of order 48.

F. Two-Walled Rectangular Corrugated Waveguide

Fig. 8 shows a two-walled corrugated rectangular waveguide. This geometry is a test case for impedance surfaces. In this geometry, the slots are not in the longitudinal direction. Thus, the cross section of this waveguide is not the same in every plane-cut normal to the direction of propagation, which means that this is not a two-dimensional problem. However, if the front surface of the corrugations is taken as impedance surface, this geometry can be solved as a 2-D problem. In the actual geometry, there is a constant number of slots per wavelength, and the ridges are assumed to be infinitely thin so that the longitudinal geometry is not a parameter in the expression of the surface impedance. With these assumptions,

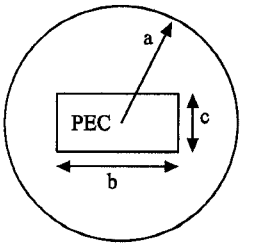

Fig. 7. Coaxial waveguide. For this example, $a = 1.0$, $b = 0.5$, and $c = 0.25$.

TABLE V
CUTOFF WAVENUMBERS FOR COAXIAL WAVEGUIDE

TM		TE	
Reference [9]	Present	Reference [9]	Present
3.8919	3.8975	1.7407	1.7404
4.1666	4.1706	3.0441	3.0464
4.4450	4.4500	4.2199	4.2175
5.2645	5.2657	4.6451	4.6127

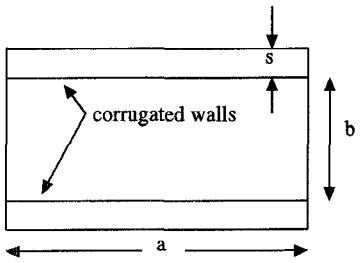

Fig. 8. Two-walled rectangular corrugated waveguide.

the surface impedance is [14]

$$Z_s = \frac{j\omega\mu}{\beta_1} \tan \beta_1 s \tag{19}$$

where $\beta_1^2 = k^2 - (n\pi/a)^2$ and n is the mode number. In (19), the quantity s is the depth of the corrugations. If $\beta_1 s$ is small when s is small, the surface impedance can be taken as mode independent so that $Z_s = j\omega\mu s$. At the surfaces of the corrugations, $y = \pm b/2$, $E_x = 0$, and $E_y \neq 0$. This boundary condition will be satisfied by hybrid electric (HE) modes (TE to x modes). At cutoff, HE modes reduce to the modes of TM to z. As a result the TM to z case can be used to compute the cutoff wavenumber of HE modes.

An analytical solution for this problem is available in [14]. The cutoff wavenumber of several modes are calculated from the exact solutions and compared to those obtained using the present method as shown in Fig. 9. In this figure, the cutoff wavenumbers are plotted versus the ratio of b/a with $s/a = 0.05$. The largest difference between the numerical and analytical results in Fig. 9 is less than 0.1%. The CFIE formulation ($\alpha = 1$) is employed in this example.

G. Dielectric-Loaded Double-Ridged Waveguide

Table VI lists the cutoff wavenumbers obtained by the present method for the dielectric-loaded double-ridged waveguide illustrated in Fig. 10(a). The matrix order is 158. The results obtained with the present method are compared to those computed using the finite element method in [3]. In [3], only certain TE modes are considered. Modes not reported in [3] are also given in Table VI.

Due to the symmetry of this waveguide, only one-quarter of the original geometry needs to be considered in the MM solution. This is illustrated in Fig. 10(b). The original problem can be subdivided into eight distinct cases: TE or TM to z with

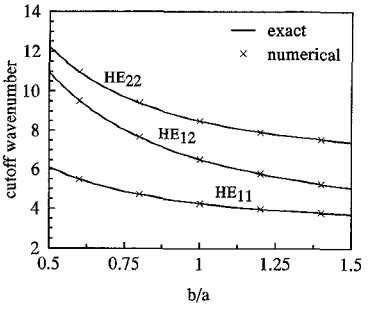

Fig. 9. Cutoff wavenumbers of two-walled rectangular corrugated waveguide.

TABLE VI
CUTOFF WAVENUMBERS FOR ORIGINAL DIELECTRIC-LOADED DOUBLE-RIDGED WAVEGUIDE

TE		TM	
Reference [3]	Present	Reference [3]	Present
0.1288	0.1291		0.6576
NA	0.3137	NA*	0.8694
NA	0.5080		0.9786
0.6190	0.6190		1.0758
0.6552	0.6550		1.1741
NA	0.6931		1.2868
NA	0.7608		1.3811
0.8890	0.8871		
NA	0.9459		
NA	1.0054		

*NA means that the published data are not available.

PEC or PMC walls at the two planes of symmetry, s and p. The modes are identified by a notation like TE(Me) that indicates a TE mode in the subdivided problem with PMC on s and PEC on p. The cutoff wavenumbers given in Table VI from [3] are for TE(Me) modes. The largest difference between our results (calculated without the use of waveguide symmetry) and those in [3] is about 1.0%.

Cutoff wavenumber results determined using waveguide symmetry are given in Table VII for TE modes. In the subdivided problem, the matrix order is 48, which is one-third of the matrix order obtained from the complete geometry. The boundary segmentation is maintained as in the original

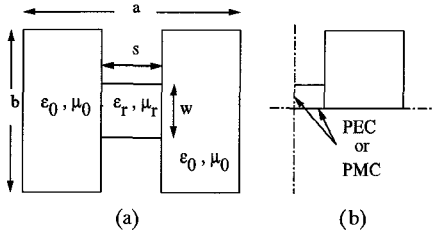

Fig. 10. (a) Dielectric-loaded double-ridged waveguide. For this example, $\mu_r = 1.0$, $\epsilon_r = 1.5$, $a = 12.70$, $b = 10.16$, $s = 2.54$, and $w = 2.79$. (b) One-quarter of the dielectric-loaded double-ridged waveguide.

TABLE VII
CUTOFF WAVENUMBERS FOR DIELECTRIC-LOADED DOUBLE-RIDGED WAVEGUIDE (ONE-QUARTER)

TE Original	TE(Me)*	TE(eE)*	TE(Mm)*	TE(Mm)*
0.1291	0.1291			
0.3137			0.3160	0.3165
0.5080		0.5116		
0.6190	0.6192	0.6193		
0.6550	0.6559			
0.6931			0.6895	0.6940
0.7608		0.7658		
0.8871	0.8894			
0.9459			0.9446	0.9446
1.0054		1.0116		

*Lowercase m or e denotes magnetic or electric wall at symmetry plane S; uppercase M or E denotes magnetic or electric wall at symmetry plane P.

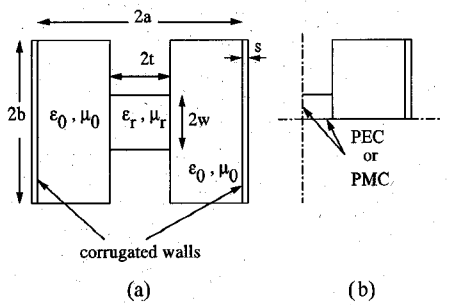

Fig. 11. (a) Two-wall corrugated dielectric-loaded double-ridged waveguide. For this example, $a = 1.0$, $b = 1.0$, and $t = 0.2$. (b) One-quarter of the two-wall corrugated dielectric-loaded double-ridged waveguide.

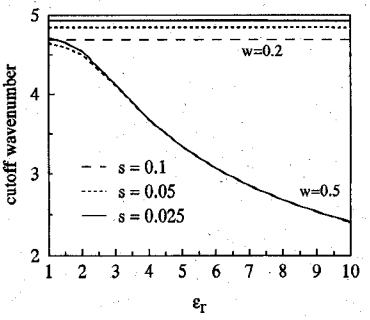

Fig. 12. Cutoff wavenumber versus the dielectric constant in a two-wall corrugated dielectric-loaded double ridged waveguide.

problem. Because the matrix order is greatly reduced in the subdivided problem compared to the original problem, the valleys around the null points of the determinant of the MM matrix are wider so that the cutoff wavenumbers are easier to locate.

H. Two-Wall Corrugated Dielectric-Loaded Ridged Waveguide

The final example was selected to have a combination of impedance and dielectric materials as well as perfect electric and magnetic conductors. This example is the two-wall corrugated dielectric-loaded ridged waveguide shown in Fig. 11(a). Here, the surface impedance is treated as in the example of Fig. 8. At the cutoff frequency, the TE to x modes reduced to the TM to z modes. Thus, the TM to z polarization is considered. Using the partitioning procedure, the problem is divided to eight distinct cases (as in the dielectric-loaded double-ridged waveguide). The partitioned waveguide is shown in Fig. 11(b). The cutoff wavenumbers of the dominant mode are plotted versus the dielectric constant with the aperture width, $2w$, and the corrugation depth, s, as the parameters in Fig. 12. When the aperture width is small, the cutoff wavenumber is not affected by the dielectric constant indicating that the waveguide is acting as two rectangular waveguides, each with one corrugated wall. When the aperture width increases, the cutoff wavenumber varies significantly with the dielectric constant, but the corrugation depth has minimal effect on the cutoff wavenumber. Note that the interior dimensions of the waveguide, a and b, are constant so that increasing the corrugation depth increases exterior dimensions of the waveguide. The cross section used to analyze the waveguide does not change with corrugation depth because the surface impedance is used to model the variation in corrugation depth.

V. Conclusions

For computation of cutoff wavenumber, a numerical technique has been successfully applied to partially dielectric filled waveguides of arbitrary cross section. This method is based on surface integral formulations and the method of moments. Polarizations TE to z and TM to z are considered separately.

Since perfect electric conductor, perfect magnetic conductor, and imperfect conductor surfaces have been considered on the conducting wall of the waveguides, techniques may be used to reduce the matrix size in the method of moments.

The impedance boundary condition is used on the imperfect conductor surfaces. The IBC is also used to simulate corrugated walls so that the equivalent currents inside the corrugated slots need not be considered. This reduces the MM matrix size.

Waveguide cross-section symmetry is also used to reduce the matrix size. The planes of cross-section symmetry are replaced by perfect electric conductor or perfect magnetic conductor walls, so that the original problem can be subdivided into several smaller problems. The cutoff wavenumbers of new geometries that use electric or magnetic conductor walls at the symmetry planes are the same as that of original geometry. Since only a part of the original geometry is considered, the matrix size is greatly reduced.

No spurious modes were observed in this work. The accuracy of the method presented here has been tested with many typical examples. In most geometries, the computed results are compared to analytical results or to published data. Excellent agreement has been achieved.

References

[1] F. L. Ng, "Tabulation of methods for the numerical solution of the hollowwave guide problem," *IEEE Trans. Microwave Theory Tech.*, vol. MTT-22, pp. 322–329, Mar. 1974.

[2] Y. Utsumi, "Variational analysis of ridged waveguides mode," *IEEE Trans. Microwave Theory Tech.*, vol. MTT-33, pp. 111–120, Feb. 1985.

[3] M. Israel and R. Miniowitz, "Hermitian finite-element method for inhomogeneous waveguides," *IEEE Trans. Microwave Theory Tech.*, vol. MTT-38, pp. 1319–1326, Sept. 1990.

[4] B. M. Rahman and J. B. Davies, "Finite-element analysis of optical and microwave waveguide problems," *IEEE Trans. Microwave Theory Tech.*, vol. MTT-32, pp. 20–28, Jan. 1984.

[5] K. Hayata, M. Koshiba, M. Eguchi, and M. Suzuki, "Vectorial finite-element method without any spurious solutions for dielectric waveguiding problems using transverse magnetic-field component," *IEEE Trans. Microwave Theory Tech.*, vol. MTT-34, pp. 1120–1123, Nov. 1986.

[6] T. Angkaew, M. Matsuhara, and N. Kumagai, "Finite element analysis of waveguide modes: A novel approach that eliminates spurious modes," *IEEE Trans. Microwave Theory Tech.*, vol. MTT-35, pp. 117–123, Feb. 1986.

[7] T. K. Sarkar, K. Athar, E. Arvas, M. Manela, and R. Lade, "Computation of the propagation characteristics of TE and TM modes in arbitrary shaped hollow waveguides utilizing the conjugate gradient method," *Electromagn. Waves Appl.*, vol. 3, pp. 143–165, Feb. 1989.

[8] C. Y. Kim, S. D. Yu, R. F. Harrington, J. W. Ra, and S. Y. Lee, "Computation of waveguide modes for waveguides of arbitrary cross-section," *IEE Proc.*, vol. 137, Pt.H, no. 2, Apr. 1990.

[9] M. Swaminathan, E. Arvas, T. K. Sarkar, and A. R. Djordjevic, "Computation of cutoff wavenumbers of TE and TM modes in waveguides of arbitrary cross sections using a surface integral formulation," *IEEE Trans. Microwave Theory Tech.*, vol. MTT-38, pp. 154–159, Feb. 1990.

[10] B. E. Speilman and R. F. Harrington, "Waveguides of arbitrary cross section by solution of a nonlinear integral equation," *IEEE Trans. Microwave Theory Tech.*, vol. MTT-20, pp. 578–585, Sept. 1972.
[11] J. R. Mautz and R. F. Harrington, "Boundary formulations for aperture coupling problems," *Arch. Elek. Ubertragung*, vol. 34, pp. 377–384, 1980.
[12] P. M. Goggans and T. H. Shumpert, "CFIE MM solution for TE and TM incident on a 2-D conducting body with dielectric filled cavity," *IEEE Trans. Antennas Propagat.*, vol. AP-38, pp. 1645–1649, Oct. 1990.
[13] W. H. Press, B. P. Flannery, S. A. Teukolsky, and W. T. Vetterling, *Numerical Recipes*. Cambridge, UK: Cambridge University Press, 1986.
[14] P. J. B. Clarricoats and A. D. Olver, *Corrugated Horns for microwave Antennas (IEE Electromagnetic Waves Series: 18)*. London, UK: Peter Peregrinus, 1984, pp. 183–188.
[15] R. F. Harrington, *Time Harmonic Electromagnetic Fields*. New York: McGraw-Hill, 1961, pp. 158–161.

Shianfeng Shu was born in Jiangsu Province, People's Republic of China, on January 28, 1968. He received the B.S. degree in electrical engineering from the University of Science and Technology of China in 1989, and the M.S. degree from the University of Mississippi in 1991.

From 1990 to 1991 he was a Research Assistant in the Department of Electrical Engineering at the University of Mississippi. He is currently employed by Formosa Plastics Corporation, USA, Livingston, NJ, His main research interests are in applied electromagnetic theory, computer-aided design, and antennas.

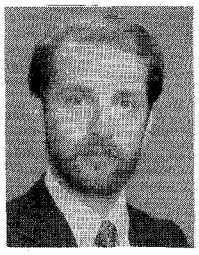

Paul M. Goggans received the B.S. M.S. and Ph.D. degrees in electrical engineering from Auburn University, Auburn, AL, in 1976, 1978, and 1990, respectively.

From 1979 to 1985 he was employed by Sandia National Laboratories, Albuquerque, NM, in the Radar Signal Analysis Division. From 1985 to 1990 he was an Instructor at Auburn University while working toward the Ph.D. degree. Upon completion of the doctoral program, he was appointed Assistant Professor in the Department of Electrical Engineering at the University of Mississippi, Oxford. His research interests include numerical solutions to the problem of electromagnetic scattering from composite bodies. Of particular interest are solutions which combined the method of moments with other methods.

Dr. Goggans is a member of Eta Kappa Nu, Phi Kappa Phi, Sigma Xi, and the IEEE Antennas and Propagation, Microwave Theory and Techniques, Electromagnetic Compatibility, and Education Societies.

Ahmed A. Kishk received the B.S. degrees in electrical engineering from Cairo University, Cairo, Egypt, in 1977, and in applied mathematics from Ain-Shams University, Cairo, Egypt, in 1980. He received the M.Eng. and Ph.D. degrees in 1983 and 1986, respectively, both from the University of Manitoba, Canada.

He is an Associate Professor at the University of Mississippi. His research interests are in the areas of numerical techniques for electromagnetic problems, microstrip antennas, and dielectric resonator antennas. He has published over 130 technical papers, presentations, and reports. He is currently an Editor of Antennas & Propagation Magazine.

Dr. Kishk is a member of Sigma Xi Society and the Electromagnetic Academy.